

Long-Range Order in Electronic Transport through Disordered Metal Films

S. Aigner,^{1,2} L. Della Pietra,² Y. Japha,³ O. Entin-Wohlman,³

T. David,³ R. Salem,³ R. Folman,³ and J. Schmiedmayer^{1,2}

¹Atominstitut der Österreichischen Universitäten, TU-Wien, Stadionallee 2, 1020 Vienna, Austria

²Physikalisches Institut, Universität Heidelberg, Philosophenweg 12, D-69120 Heidelberg, Germany

³Department of Physics, Ben-Gurion University of the Negev, P.O. Box 653, Be'er-Sheva 84105, Israel

Ultracold atom magnetic field microscopy enables the probing of current flow patterns in planar structures with unprecedented sensitivity. In polycrystalline metal (gold) films we observe long-range correlations forming organized patterns oriented at $\pm 45^\circ$ relative to the mean current flow, even at room temperature and at length scales orders of magnitude larger than the diffusion length or the grain size. The preference to form patterns at these angles is a direct consequence of universal scattering properties at defects. The observed amplitude of the current direction fluctuations scales inversely to that expected from the relative thickness variations, the grain size and the defect concentration, all determined independently by standard methods. This indicates that ultracold atom magnetometry enables new insight into the interplay between disorder and transport.

Thin metal films are the classic environment for studying the effect of geometric constraints [1, 2] and crystal defects [3, 4] on the transport of electrons. In a perfectly straight long wire that is free from structural defects, a direct current (DC) strictly follows the wire direction and creates a magnetic field in the plane perpendicular to the wire. An obstacle may locally change the direction of the current and consequently locally rotate the magnetic field close to the wire by an angle β in a plane parallel to the plane of the thin film wire.

Ultracold atom magnetometry [5, 6] on atom chips [7, 8, 9] allows for the sensitive probing of this angle β (and its spatial variation) with μrad (μm) resolution. Compared to scanning probes having a μm scale spatial resolution and 10^{-5}T sensitivity, or superconducting quantum interference devices (SQUIDs) having 10^{-13}T sensitivity but a resolution of tens of μm , ultracold atom magnetometry has both high sensitivity (10^{-10}T) and high resolution (several μm) [6]. In addition, ultracold atoms enable high resolution over a large length scale (mm) in a single shot. This enables the simultaneous observations of microscopic and macroscopic phenomena, as described in this work.

Using cold atoms just above the transition to Bose-Einstein Condensation (BEC), we apply ultracold atom magnetometry to study the current deflection in three different precision-fabricated polycrystalline gold wires with a rectangular cross section of $200\mu\text{m}$ width and different thicknesses and crystalline grain sizes, as summarized in Table I [10]. Choosing the wire length along x , its width along y and thickness along z , Fig. 1 shows the maps of the angular variations $\beta(x, y, z_0) = \delta B_x(x, y, z_0)/B_y$ of the magnetic field created by a current of 180 mA flowing along the wire, measured at $z_0 = 3.5\mu\text{m}$ above its center (far from the edges).

Even though at ambient temperature scattering by lattice vibrations (phonons) quickly diffuses the electronic motion, long-range correlations (tens of μm) in the current flow patterns can be seen. This is surprising as effects of static defects are usually observed only on a

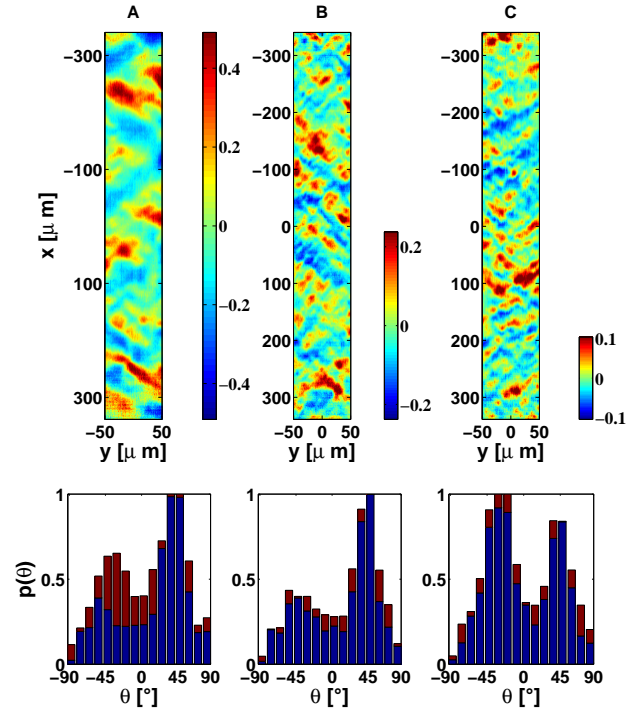


FIG. 1: (top) Magnetic field angle fluctuations β [mrad] above three (A-C) different polycrystalline gold films described in Table I. These fluctuations are due to variations in the direction of the current flow and are thus sensitive to δJ_y . The appearance of $\pm 45^\circ$ patterns is clearly observable, and reflects a correlated scattering of the electrons. (bottom) Quantification of the angular pattern by the normalized angular power spectral density $p(\theta)/\max(p)$. The red bars indicate the error.

length-scale of several nanometers [11, 12]. We observe clear patterns of elongated regions of maximal current flow deviations β inclined by about $\pm 45^\circ$ to the mean current flow direction. This angular preference is present in all the measurements, independent of wire thickness or grain size. This preference can be quantified by the normalized angular power spectra $p(\theta) = \int dk k |\beta(k, \theta)|^2$

wire	A	B	C
thickness H (μm)	2.08	0.28	0.28
grain size (nm)	60-80	30-50	150-170
resistivity at 296K ($\mu\Omega\cdot\text{cm}$)	2.73	3.1	2.77
resistivity at 4.2K ($\mu\Omega\cdot\text{cm}$)	0.094	0.316	0.351
atom temperature (nK)	286 ± 15	173 ± 2	92 ± 7
measurement height (μm)	3.5 ± 0.4	3.4 ± 0.3	3.7 ± 0.4
δz_+^{rms} (AFM) (nm)	9.4	3.5	3.1
δz_+^{rms} (WLI) (nm)	1.31	0.42	0.48
$\delta z_+^{\text{rms}}/H$ (WLI) ($\times 10^{-3}$)	0.629	1.500	1.714
β_{rms} (mrad)	0.168	0.0715	0.0388
β_{pp} (mrad)	0.4	0.2	0.1
λ_β (μm)	77	46	48

TABLE I: Properties of the wires under investigation. All measurements were done on the chip used for the cold atom experiment except for the low temperature resistivity which was measured on a duplicate chip made with an identical (simultaneous) fabrication process. (AFM: Atomic force microscope; WLI: ZYGO white light interferometer)

of the magnetic field patterns, where \mathbf{k} is the wavevector of the Fourier transform of the measured $\beta(x, y)$ (Fig. 1).

We observe significant difference in the magnitude and spectral composition of the magnetic field variations above wires with different thicknesses. Table 1 summarizes the main observations and wire properties. The magnitude of β scales contrary to the surface corrugations when compared to the thickness; the thinner films ($H = 280$ nm) have the largest relative thickness variations but show the smallest current directional variations. Moreover, the thin wire with the large grains (grain size 150-170 nm) shows the smallest variations ($\beta_{\text{rms}} = 39 \mu\text{rad}$), much too small to be explained by the measured top surface roughness $\delta z_+^{\text{rms}}/H = 1.7 \times 10^{-3}$ of the gold film.

The observed magnetic field variations caused by the current direction variations are orders of magnitude smaller than the ones reported in studies of 'fragmentation' of cold atom clouds on atom chips (for a review see [9]). These previously reported fragmentation measurements can be fully explained by corrugations in the wire edges [13, 14]. In the present study the effects caused by the wire edge roughness are strongly suppressed by the much improved fabrication [10, 15], and the flat wide wire geometry where the ratio between the distance to the wire surface and to the wire edge is very high [16].

In order to analyze the underlying mechanism for the current direction deviations we consider a thin film (conductivity σ_0) in the $x - y$ plane with a regular current $J_0 \hat{x} = \sigma_0 \mathbf{E}^{(0)}$, where the electric field $\mathbf{E}^{(0)}$ is in the \hat{x} direction. We consider the effect of small fluctuations in the conductivity $\delta\sigma(\mathbf{x})$ on the current flow.

The current flow around a circular defect (Fig. 2A,B) generates a dipole field with a transverse component $E_y^{(1)} \propto \sin 2\theta$, causing the current field to be repelled

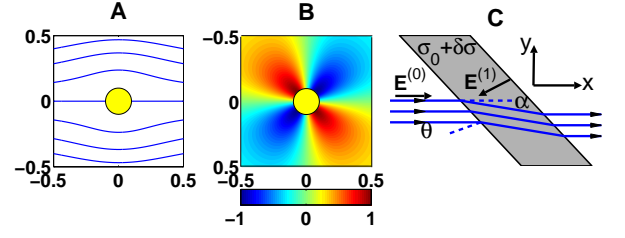


FIG. 2: (A) Current scattering by circularly symmetric (disk) local conductivity variations $\delta\sigma < 0$. (B) The transverse (\hat{y}) component of the current is proportional to $\sin 2\theta$. (C) Direction change of a current flow due to a conductivity step defect inclined by an angle θ relative to the current flow direction \hat{x} . The conductivity is σ_0 everywhere except in the shaded area, where it is $\sigma_0 + \delta\sigma$ ($\delta\sigma > 0$ in this example). Again, the electron scattering amplitude is proportional to $\sin 2\theta$.

from (for $\delta\sigma < 0$) or attracted to (for $\delta\sigma > 0$) the defect and a 45° pattern in the transverse current flow forms.

A second illustration is a conductivity step ($\delta\sigma$) inclined by an angle θ to the current flow direction (Fig. 2C). The resulting current density fluctuation is:

$$\delta\mathbf{J} = J_0 \frac{\delta\sigma}{\sigma_0} (\sin^2 \theta \hat{x} - \cos \theta \sin \theta \hat{y}). \quad (1)$$

The transverse current component J_y is again proportional to $\sin 2\theta$, which is maximal for conductivity steps inclined by $\theta = \pm 45^\circ$.

In a metal film, we expect to find a random pattern of conductivity fluctuations $\delta\sigma(\mathbf{x})$. It can be constructed from a random spatial distribution of the above basic elements: microscopic circular defects or macroscopic conductivity steps of different angles.

For a general quantitative analysis we expand an arbitrary distribution $\delta\sigma(\mathbf{x})$ in a Fourier series of plane waves of the form $\delta\sigma(\mathbf{x}) = \delta\sigma_{\mathbf{k}} \sin(\mathbf{k} \cdot \mathbf{x} + \phi)$, where $\mathbf{k} = (k_x, k_y) = k(\cos \theta_{\mathbf{k}}, \sin \theta_{\mathbf{k}})$ and ϕ is an arbitrary phase. Each plane wave contributes to the current fluctuation angle $\alpha = \delta J_y / J_0$ according to Eq. 1, giving $\alpha(\mathbf{k}) \approx -\sin 2\theta_{\mathbf{k}} (\delta\sigma_{\mathbf{k}} / 2\sigma_0)$, and resulting in the observed 45° pattern.

The resulting magnetic field angle fluctuations at height z above the wire is directly related to the current fluctuations by

$$\beta(\mathbf{k}, z) \approx e^{-kz} \alpha(\mathbf{k}) \approx -\frac{1}{2} e^{-kz} \frac{\delta\sigma_{\mathbf{k}}}{\sigma_0} \sin 2\theta_{\mathbf{k}}, \quad (2)$$

which exhibits the same angular dependence. The exponential term e^{-kz} represents a resolution limit, such that the effect of current changes on a length scale smaller than $2\pi z$ are suppressed in the spectrum of the magnetic field fluctuations. Starting from random conductivity fluctuations with a non-white spatial frequency distribution the angular dependence $\sin 2\theta$ will emerge, giving rise to the observed $\pm 45^\circ$ preference. We have simulated such random models and the observable β forms very similar 2D maps as in Fig. 1.

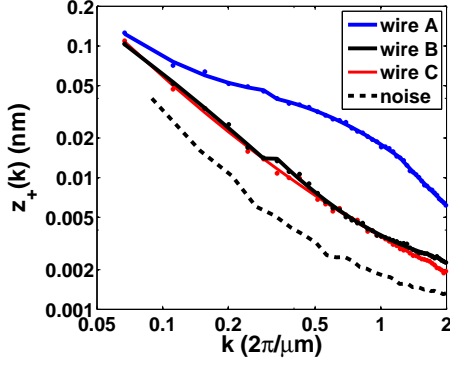


FIG. 3: Radial spectrum of the top surface corrugations $|\delta z_+(k)| = \sqrt{(2\pi)^{-1} \int d\theta |\delta z_+(k, \theta)|^2}$ for the three wires measured using a white-light interferometer. Note the significant difference between wire **A** and wires **B**, **C**. (dashed) Measurement noise level calculated by averaging over many partly overlapping images

The variations $\delta\sigma(\mathbf{x})$ in the conductivity σ in a thin metal film are caused by contributions from two physical origins: bulk conductivity variations in the metal, and variations in the boundaries, namely variations in the thickness H of the film $\delta H(\mathbf{x})$ leading to a change in the conductivity per unit area $\delta\sigma = \sigma_0 \delta H/H$.

In order to investigate whether the observed current flow deviations are related to corrugations in the top surface of the wire, we have measured the surface topography of the wires using a white-light interferometer. No angular preference inherent in the structure of the wires was found. Consequently, the angular pattern in the magnetic field variations presented in Fig. 1 must be a pure property of the scattering mechanism of the current flow by the wire defects, as outlined above. More so, when we calculate the two dimensional magnetic field at $3.5\mu\text{m}$ above the surface, using the white-light interferometry measurements and the assumption $\delta H(\mathbf{x}) = \delta z_+(\mathbf{x})$, we could not find a reasonable fit between the latter and the magnetic mapping done by the atoms (Fig. 1). A detailed analysis of the top surface corrugations δz_+ (Fig. 3) shows that they are significantly larger for the thick film compared to the two thin films, especially at short length scales.

To quantify our findings, we compare the power spectra of the measured magnetic field variations to those calculated from several models based on the measured top surface variations, an assumed bottom surface roughness, and possible inhomogeneities in the bulk conductivity (Fig. 4).

We start with the two thin wires: **B** and **C**. The measured power spectra of the magnetic field variations are significantly lower (by two orders of magnitude for large wavelengths) than predictions based on a model with a flat bottom surface ($\delta H = \delta z_+$). If we assume that the top surface exactly follows the bottom surface

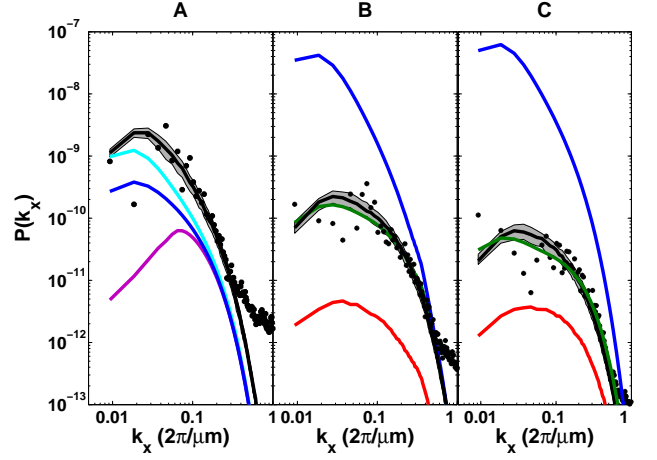


FIG. 4: Comparison of surface and bulk model calculations (lines) with the measured power spectrum $P(k_x) = \sum_{k_y} |\beta(k_x, k_y)|^2$ of the magnetic field angle β along the x direction above the three wires (points). (blue) top surface δz_+ as in Fig. 3 with flat bottom surface $\delta z_- = 0$. (red) top surface follows bottom surface $\delta z_+ = \delta z_-$ (i.e. no thickness variations). (green) Partially correlated top and bottom surfaces for wires **B** and **C**. For the thick wire **A** we assume $\delta z_-(k)$ as in wire **B**, which is correlated (purple) or uncorrelated (light blue) with the top surface. The latter gives the closest estimate for the experimental data, but gives β_{rms} which is only about half of the measured value. (black) a fit to a model assuming bulk conductivity fluctuations. The shaded area represents a one-standard-deviation range obtained by varying the relative phases of different spectral components $\delta\sigma(k_x, k_y)$.

($\delta z_+ = \delta z_-$), a lower bound on the influence of the surface on magnetic field fluctuations can be obtained, as this configuration produces vertical currents whose contribution to the longitudinal magnetic field, to which our experiment is sensitive, is very small. The measured data is in between these two cases.

A fair fit of the measured spectrum for the thin wires is obtained if we assume that the top surface partially follows the large-wavelengths fluctuations of the bottom surface while independent fluctuations of the top surface exist in the shorter scale. For such a model we assume $\delta z_-(k) \approx \delta z_+(k) e^{-(k/k_0)^2}$. Note that the resulting average thickness variations are extremely small $|\delta H^{rms}| = |\delta z_+^{rms} - \delta z_-^{rms}| < 1\text{\AA}$. This value of δH^{rms} refers to length scales longer than $1\mu\text{m}$, while much larger surface variations were measured on the scale of the grains using the AFM (see Table I).

The situation is different for the thick wire **A** ($H = 2\mu\text{m}$). Models assuming a flat bottom surface ($\delta H = \delta z_+$) and models assuming a corrugated bottom surface δz_- with a spectrum similar to that of wire **B** and no correlations with the top surface, both underestimate the measured magnetic field variations.

The difference between the surface models and the measured data of wire **A** can be attributed to fluctuations

in the bulk conductivity. A model taking the maximal contribution of surface roughness (uncorrelated top and bottom surfaces) into account gives the minimal required contribution of the bulk conductivity fluctuations. If we apply the same minimal bulk conductivity fluctuations as obtained from wire **A** to the two thin wires **B** and **C**, they overestimate the measured magnetic field fluctuations substantially for both wires and give a different spectral shape. This indicates that the bulk conductivity of the thinner wires should be more homogeneous than that of the thick wire.

A more homogeneous bulk conductivity in the thin wires, however, appears to be contradictory to the fact that the low temperature resistivity is smaller for the thick wire than for the thin wires (Table 1). Nevertheless, we note that this resistivity is mainly determined by the small-scale properties of the wire (on the order of the grain size or less) and by surface scattering, while the magnetic field variations probe the conductivity inhomogeneities at a larger scale and provide complementary information that would not be available by standard methods.

Our analysis furthermore suggests that the differences in the length scale λ_β of the variation in β as seen in Fig. 1 and quantified in Table 1, may originate from the fact that conductivity variations in the thin wires coming from thickness variations are suppressed at long length scales due to top and bottom surface correlations. In contrast, conductivity variations in the thick wire originate at all scales from a combination of thickness variations due to uncorrelated top and bottom surfaces and a dominant contribution of bulk conductivity inhomogeneity.

Our study is the first direct application of ultracold atoms as a probe for solid state science. The exceptional sensitivity of the ultracold atom magnetic field microscope [5, 6] allowed us to observe long-range patterns of the current flow in a disordered metal film. The preference of features with angles around $\pm 45^\circ$ in the measured angular spectrum of the current flow fluctuations is due to the universal scattering properties at defects. A detailed quantitative analysis shows that the observed current directional fluctuations at different wires exhibits significantly different and unexpected properties due to different physical origins. This clearly demonstrates the power of the ultracold atom magnetic field microscope to study details of the current flow in conductors, and its ability to unveil previously inaccessible information. This may be expected to stimulate new studies on the interplay between disorder and coherent transport in a variety of systems ranging from high- T_c superconductors [17] to 2D electron gases [18] and nano-wires [19].

We thank the team of the Ben-Gurion University Weiss Family Laboratory for Nanoscale Systems for the fabrication of the chip and Jürgen Jopp of the Ben-Gurion University Ilse Katz Center for Nanoscale Science for assisting with surface measurements. R.F. thanks Yoseph (Joe) Imry and Sir Aaron Klug for their continued support. We acknowledge the support by the FWF, the DFG, the German Federal Ministry of Education and Research (DIP), the European Commission through the Integrated Project FET/QIPC "SCALA" and the RTN "AtomChips", the American-Israeli Foundation (BSF) and the Israeli Science Foundation.

-
- [1] E. H. Sondheimer, *Adv. Phys.* **1**, 1 (1952).
 - [2] R. G. Chambers, *Proc. R. Soc. London, Ser. A* **202**, 378 (1950).
 - [3] A. F. Mayadas, M. Shatzkes, *Phys. Rev. B* **1**, 1382 (1970).
 - [4] R. Landauer, *IBM J. Res. Dev.* **1**, 223 (1957).
 - [5] S. Wildermuth *et al.*, *Nature* **435**, 440 (2005).
 - [6] S. Wildermuth *et al.*, *Appl. Phys. Lett.* **88**, 264103 (2006).
 - [7] R. Folman, P. Krüger, J. Schmiedmayer, J. Denschlag, C. Henkel, *Adv. At. Mol. Opt. Phys.* **48**, 263 (2002).
 - [8] J. Reichel, *Appl. Phys. B* **74**, 469 (2002).
 - [9] J. Fortagh, J. C. Zimmermann, *Rev. Mod. Phys.* **79**, 235 (2007).
 - [10] The chip was fabricated at The Weiss Family Laboratory for Nano-Scale Systems at Ben-Gurion University, Israel, www.bgu.ac.il/nanofabrication.
 - [11] W. Steinhögl, G. Schindler, G. Steinlesberger, M. Engelhardt, *Phys. Rev. B* **66**, 075414 (2002).
 - [12] M. A. Schneider, M. Wenderoth, A. J. Heinrich, M. A. Rosentreter, R. G. Ulbrich, *Appl. Phys. Lett.* **69**, 1327 (1996).
 - [13] D.-W. Wang, M. D. Lukin, E. Demler, *Phys. Rev. Lett.* **92**, 076802 (2004).
 - [14] T. Schumm *et al.*, *Euro. Phys. J. D* **32**, 171 (2005).
 - [15] S. Groth *et al.*, *Appl. Phys. Lett.* **85**, 2980 (2004).
 - [16] P. Krüger *et al.*, arXiv:cond-mat/0504686; P. Krüger *et al.*, *Phys. Rev. A* **76**, 063621 (2007).
 - [17] D. A. Bonn, *Nature Physics* **2**, 159 (2006).
 - [18] S. Ilani, A. Yacoby, D. Mahalu, H. Shtrikman, *Science* **292**, 1354 (2001).
 - [19] J. Feist *et al.*, *Phys. Rev. Lett.* **97**, 116804 (2006).